SCIENTIFIC REPORTS

OPEN

SUBJECT AREAS:
ELECTRONIC PROPERTIES AND MATERIALS
TWO-DIMENSIONAL MATERIALS
ELECTRONIC DEVICES

Received
16 July 2014

Accepted
14 November 2014

Published
3 December 2014

Correspondence and requests for materials should be addressed to G.E. (g.eda@nus.edu.sg)

* These authors contributed equally to this work.

Charge transport in ion-gated mono-, bi-, and trilayer MoS_2 field effect transistors

Leiqiang Chu[1,2]*, Hennrik Schmidt[1,2]*, Jiang Pu[4], Shunfeng Wang[1,2], Barbaros Özyilmaz[1,2], Taishi Takenobu[4,5,6] & Goki Eda[1,2,3]

[1]Graphene Research Centre, National University of Singapore, 6 Science Drive 2, Singapore 117546, [2]Department of Physics, National University of Singapore, 2 Science Drive 3, Singapore 117542, [3]Department of Chemistry, National University of Singapore, 3 Science Drive 3, Singapore 117543, [4]Department of Advanced Science and Engineering, Waseda University, Tokyo 169-8555, Japan, [5]Department of Applied Physics, Waseda University, Tokyo 169-8555, Japan, [6]Kagami Memorial Laboratory for Material Science and Technology, Waseda University, Tokyo 169-0051, Japan.

Charge transport in MoS_2 in the low carrier density regime is dominated by trap states and band edge disorder. The intrinsic transport properties of MoS_2 emerge in the high density regime where conduction occurs via extended states. Here, we investigate the transport properties of mechanically exfoliated mono-, bi-, and trilayer MoS_2 sheets over a wide range of carrier densities realized by a combination of ion gel top gate and SiO_2 back gate, which allows us to achieve high charge carrier ($>10^{13}$ cm^{-2}) densities. We discuss the gating properties of the devices as a function of layer thickness and demonstrate resistivities as low as 1 kΩ for monolayer and 420 Ω for bilayer devices at 10 K. We show that from the capacitive coupling of the two gates, quantum capacitance can be roughly estimated to be on the order of 1 μF/cm^2 for all devices studied. The temperature dependence of the carrier mobility in the high density regime indicates that short-range scatterers limit charge transport at low temperatures.

Two-dimensional (2D) crystals of layered transition metal dichacogenides (TMD) have gained significant interest due to their unique physical properties[1,2]. Molybdenum disulfide (MoS_2), a semiconducting compound traditionally known for its lubricating properties, has been intensively investigated in its 2D crystalline form in the past few years. Field effect transistors of monolayer MoS_2 have shown remarkable characteristics with low off-current due to excellent gate electrostatics[3]. Recent studies on the implementation of MoS_2 and other semiconducting TMDs into integrated circuits[4–7] and optoelectronic devices[8–10] highlight their potential in future applications.

Electrostatically controlled switching and charge transport in mono- and few-layer MoS_2 devices are strongly influenced by various effects such as metal contacts[11,12], interface traps[13–15], charged impurities[3,13,15,16], dielectric environment[3,4,6,17,18], and structural defects[15,19–23] in the material. The contribution of these effects varies with the gate bias in a complex manner. At low gate biases near the sub-threshold region, the device resistance is strongly dominated by Schottky barriers at the metal contacts[11], band edge disorder and mid-gap states[13,21,23–25], which originate from structural defects, charge traps at the MoS_2/SiO_2 interface, and surface adsorbates[13,14]. At higher charge densities where the channel conductivity exceeds e^2/h, conduction occurs via band-like carrier transport[18,21,26,27]. In this regime, charged impurities, defects, and surface-optical phonons[28] limit charge carrier mobility in 2D MoS_2. All recent studies show that low temperature mobility of mono- and bilayer MoS_2 falls substantially below theoretically predicted values[29,30], suggesting that there is significant room for improvement in the device performance.

The use of high-κ dielectrics, such as HfO_2[3,18,31] and Al_2O_3[17,32], as an encapsulating layer and gate barrier has been reported to be effective in enhancing carrier mobility, potentially due to dielectric screening of charged impurities and suppression of homopolar optical phonon modes[18,33]. The high-κ gate dielectric also allows access to the high density regime where transport is band-like and the intrinsic properties of the material can be investigated. In order to achieve even higher charge densities, ionic gating has been used in different 2D materials[34–39]. Previous studies using polymer electrolyte[40], ionic liquid[27,38,41,42], and ion gels[43] have demonstrated effective switching and high doping levels of up to ~10^{14} cm^{-2} in few-layer MoS_2 devices[42,43] to realize flexible transistors[43], stable p-n junctions[35,41,44], light emitting devices[32,35,44], and superconductivity[27].

In this article, we report on the low temperature transport characteristics of mono-, bi-, and trilayer MoS_2 devices in the high doping regime using ion gel gating. We show that large capacitive coupling of the ion gel in

conjunction with additional electrostatic control by the back gate allows systematic investigation of charge transport over a wide range of carrier densities. Resistivities as low as 1 kΩ and 420 Ω are realized in highly doped mono- and bilayer MoS_2 at low temperature, respectively. From the capacitive coupling of the two gates, we estimate the quantum capacitance, which is a measure of the density of states in these materials. Further analysis of the temperature- and density-dependent field effect mobility reveals that short-range scatterers severely limit carrier mobility at low temperatures in all these devices.

Results

The thickness of the exfoliated flakes is estimated by optical contrast and then further confirmed by the peak separation between the A_{1g} and $E_{2g}{}^1$ peaks in the Raman spectrum[45]. In agreement with previous studies[13], the peak separation was found to be 18.3 cm^{-1}, 21.2 cm^{-1}, and 23.1 cm^{-1} for monolayer (1 L), bilayer (2 L), and trilayer (3 L) samples, respectively. The optical images of the samples covered with a thin layer of ion gel are shown in figure 1a (see methods section for details). Figure 1b shows the transfer curves of mono-, bi-, and trilayer devices as a function of the top gate voltage (V_{tg}) applied to the ionic gate at room temperature. For bilayer and trilayer devices, both electron and hole branches are observed at positive and negative gate voltages, respectively, demonstrating the wide tunability of the chemical potential achieved by ion gel. The monolayer device only shows the electron branch in the top gate bias window studied due to its large band gap.

Assuming that the variation of the electrostatic potential is negligible, the bandgap of bilayer and trilayer samples can be roughly estimated to be 1.63 eV and 1.32 eV from the threshold voltage difference for the electron and hole branches of the transfer curve (Supplementary Information, Figure S3)[35,39,41]. These values are consistent with the optical gap previously measured by photoluminescence spectroscopy[46]. Figure 1d displays the temperature dependent transconductance of a bilayer device, obtained by sweeping the top gate voltage (4.5 mV/s) at a fixed temperature. Below $T \sim 210$ K, the top gate modulation becomes negligible, suggesting the freezing of the ions in the gel matrix. This immobilization of ions allows us to achieve stable high doping in the channel and fine control of the carrier density by the back gate below this temperature.

The dual gating behavior of the devices was studied by cooling them below the critical freezing point at a fixed top gate voltage and measuring the transfer characteristics by back gate sweeps at various temperatures. To study the device over a wide range of carrier densities, the sample was brought to room temperature and the top gate voltage was set to a desired value and held until the displacement current was negligible. The sample was then cooled below the freezing point of the ion gel for measurements. The above procedure was repeated with different top gate biases. Figures 2a–c show the back gate transfer characteristics of the devices at different top gate biases. At negative V_{tg}, transitions from the insulating to the conducting state can be observed with on-off ratios of $>10^5$ for all devices. The off-state current was limited by the gate leakage current, which was typically below 100 pA at temperatures below 200 K (See Supplementary Figure S7). It is worth noting that all samples exhibit

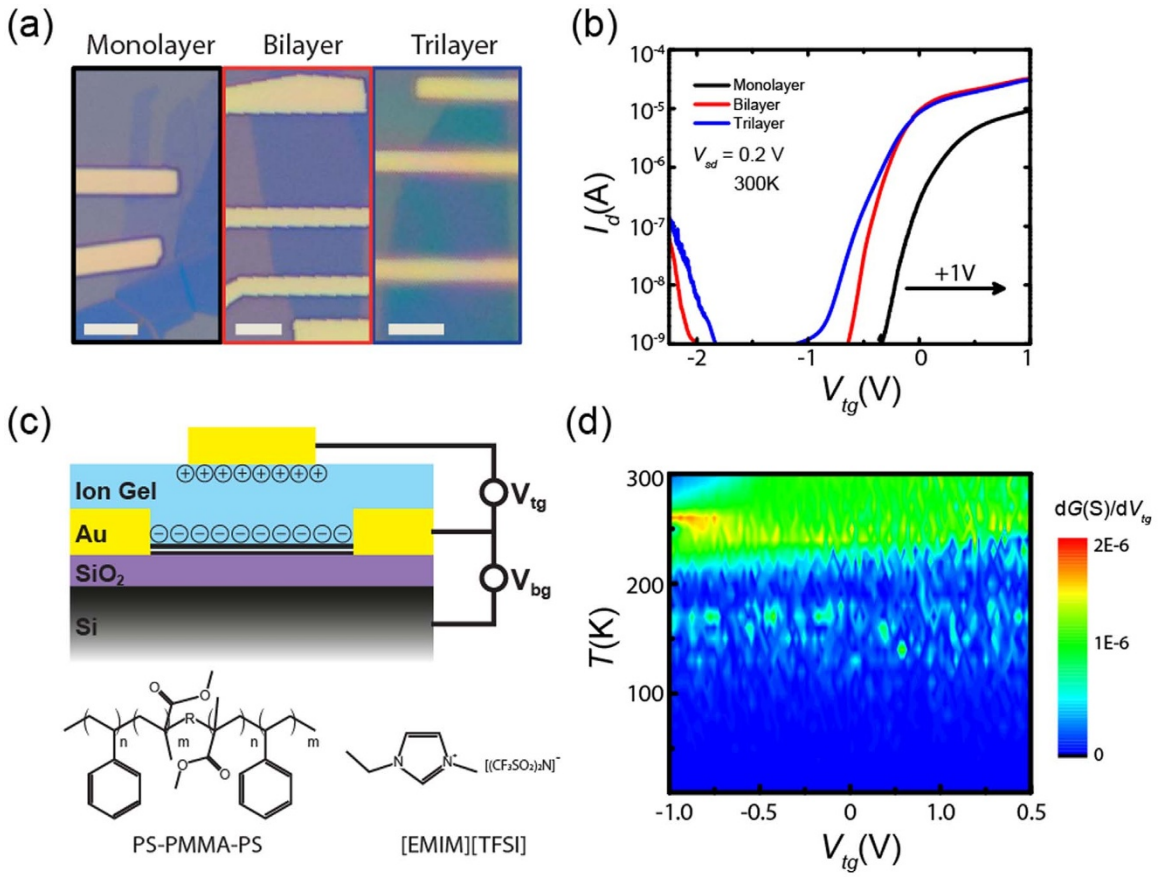

Figure 1 | Ionic gating of MoS_2 devices. (a) Optical images of mono-, bi-, and trilayer MoS_2 transistors covered with ion gel. The scale bars is 5 μm. (b) Ambipolar field-effect characteristics at room temperature. The curve for the monolayer sample is shifted by 1 V to the left for clarity. (c) Schematic illustration of a dual gated transistor and chemical structures of the copolymer and the ionic liquid used as the top gate. (d) Transconductance of a bilayer device while sweeping V_{tg} at a fixed temperature. Below ~200K, the ions are frozen out and top gate variations have no effect on the sample's conductance.

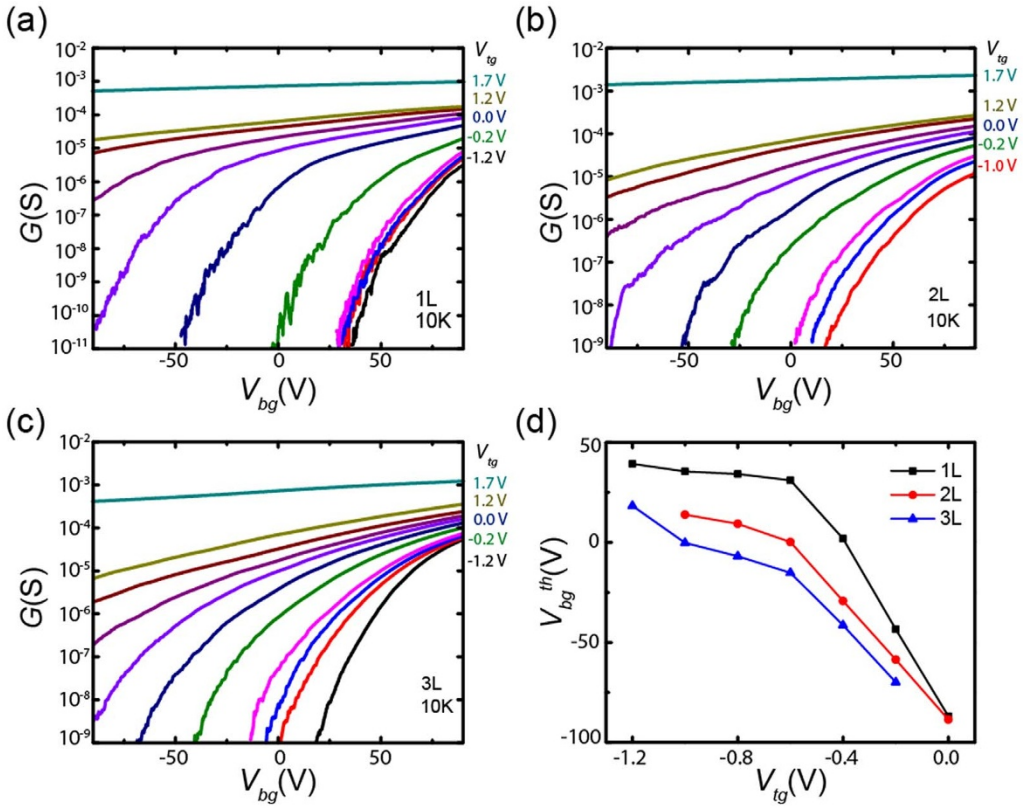

Figure 2 | Shift of threshold voltages. (a–c) Channel conductivity as a function of V_{bg} at different V_{tg} (−1.2 V, −1.0 V, … 1.0 V, 1.2 V, 1.7 V) for 1–3 L MoS_2 devices at 10 K. (d) The threshold voltage obtained from the cutoff in (a–c) as a function of V_{tg}. For positive V_{tg}, V_{bg}^{th} cannot be extracted since the sample is always in the on-state.

low sheet resistivity (<1 kΩ) at large top gate bias and low temperature. These values are among the lowest reported for monolayer and bilayer MoS_2 so far.

The threshold back gate voltage V_{bg}^{th}, which we defined here to be the bias voltage required to achieve a critical device current of 100 pA, shifts towards negative gate bias with increasing top gate voltage as shown in Figure 2d. Note that for positive top gate voltages the devices remain in the conducting state for all back gate biases. It can also be seen that the shift of V_{bg}^{th} is non-monotonous with an apparent change in the slope at around $V_{tg} = -0.6$ V. We attribute this behavior to different capacitive coupling of the top and back gate with shift in E_F and the corresponding changes in the quantum capacitance[34] C_q of MoS_2. The total top gate capacitance between ion gel and MoS_2 channel C_{tot}^{top} can be described as a series connection of C_q, which is proportional to the density of states (DOS) of the material, and the geometric capacitance of the ion gel C_{ig}. Similarly, the back gate capacitance C_{tot}^{back} can be described as quantum capacitance and the oxide capacitance C_{ox} in series. Ignoring screening effects, the top and back gate capacitances are given by:

$$C_{tot}^{top} = \left(\frac{1}{C_q} + \frac{1}{C_{ig}}\right)^{-1}$$

$$C_{tot}^{back} = \left(\frac{1}{C_q} + \frac{1}{C_{ox}}\right)^{-1}$$

Here, we can consider two regimes depending on the relative magnitude of the capacitances. When the channel is depleted and E_F lies in the band gap, C_q is very small due to the low density of mid-gap states[39]. This results in $C_q \ll C_{ig}$ and thus $C_{tot}^{top} \sim C_q$. Note that C_{tot}^{back} is affected by the same effect, but to a lesser extent because C_{ox} is intrinsically small. As a result, the ratio between c_{tot}^{top} and c_{tot}^{back} remains low. In the other limit, when the sample is strongly doped and E_F is in the conduction band, C_q significantly increases such that c_{tot}^{top} has contributions from both C_q and C_{ig} while $c_{tot}^{back} \sim C_{ox}$. In this regime, the channel conductivity is much more efficiently tuned by the top gate bias as expected from the large capacitance of the ion gel. Thus, the ratio between c_{tot}^{top} and c_{tot}^{back} increases with increasing top gate voltage due to increase in C_q.

In the following, we analyse the results in the high doping regime. Figures 3a–c show the color-coded map of the channel conductivity as a function of top and back gate biases. As indicated by the black dashed lines along constant conductivity, the top gate is 50 to 100 times more efficient compared to the back gate. The ratios $\Delta V_{bg}/\Delta V_{tg}$, where ΔV_{bg} and ΔV_{tg} denote the corresponding gate voltage difference to achieve the same change in conductivity in the metallic regime, are obtained from the slopes of the dashed lines in Figure 3. This ratio is determined to be ~86 for monolayer, ~64 for bilayer and ~43 for trilayer device.

In order to show the full range of conductivity accessible by varying the two voltages, we offset the back gate transfer curves along the horizontal axis to highlight their linear (i.e. mobility saturation) behavior (Figure 4a and b). The insets show the transition from insulating to metallic conduction regimes where the temperature coefficient changes sign[18]. The crossover occurs at $V_{bg} \sim 80$ V and $V_{tg} = 0$ V for monolayer and $V_{bg} \sim 25$ V and $V_{tg} = 0$ V for bilayer. In accordance with the previous results[18,26,27] the crossing points are at resistances on the order of h/e^2. Above the crossover point, conductivity decreases with increasing temperature, indicating phonon limited, metal-like transport. At lower charge carrier densities, increasing conductivity with increasing temperature suggests thermally activated transport and conduction by variable range hopping[13,21,23–25]. As can be seen from Figure 4b, ionic gating allows

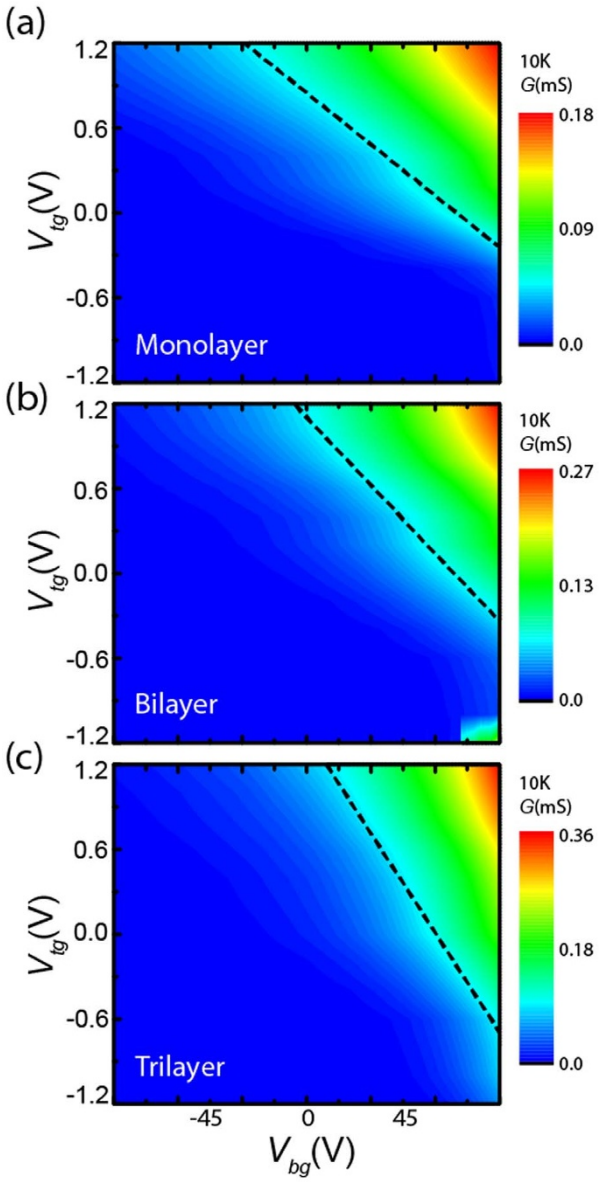

Figure 3 | Gate coupling for different number of layers. Color-coded map of the dual gate characteristics for (a) monolayer, (b) bilayer and (c) trilayer MoS_2. After setting the top gate voltage at room temperature and cooling the sample down to $T = 10$ K, the back gate bias was varied. The dashed black lines highlight constant conductivity just above the onset of conduction.

access to conduction regimes far beyond the crossover point where transport properties remains largely unexplored.

Field effect mobility and its dependence on carrier density and temperature offer insight into the fundamental transport properties of MoS_2[47]. The gate bias and temperature dependence of the field effect mobility ($\mu_{FE} = (1/C_{ox})^* d\sigma/dV_{bg}$, where $C_{ox} = 11.5$ nF/cm^2 is the back gate capacitance and σ is the channel conductivity) for mono- and bilayer MoS_2 is shown in Figures 4c–f. The mobility initially increases, and eventually saturates to a constant value at with increasing voltages. The mobility saturation can also be seen as a function of temperature below 30 K (Figure 4e and f). Note that the mobility becomes independent on both carrier density and temperature in this regime. The saturation values are about 230 cm^2/Vs, 450 cm^2/Vs, and 820 cm^2/Vs for 1, 2, and 3 L devices, respectively (see Supplementary Information for 3 L device data).

Discussion

The difference in the gate coupling ratio for 1–3 L devices can originate from various effects, such as the superposition of the two gate fields, changes of dielectric constants, different gate separation, and changes of C_{ig} or C_q as a function of layer thickness. Using a simple relationship $C_{tot}^{top}\Delta V_{tg} = C_{tot}^{back}\Delta V_{bg}$ from the capacitor model and assuming an ion gel capacitance[43] to be $C_{ig} = 10.7$ μF/cm^2, we estimate the quantum capacitance of mono-, bi-, and trilayer MoS_2 to be 1.0 μF/cm^2, 0.8 μF/cm^2, and 0.5 μF/cm^2, respectively. These are rough estimates but are on the same order of magnitude as the theoretical prediction[48]. The trend contradicts the expectation that DOS increases with increasing thickness[49], suggesting that ionic gate is effective only for the top layer, which is in direct contact with the gel. Consequently, two parallel channels that are independently controlled may be formed in multilayers. More accurate measurement of the quantum capacitance requires precise measurement of C_{ig}. (see Supplementary Information for Hall measurement results).

The mobility saturation shown in Figure 4 agrees with the earlier studies and indicates that at low temperatures and in the high carrier density regime, charge transport in these devices is dominated by short-range scattering[21]. The short-range scatterers may be structural defects such as sulfur vacancies and charged impurities which are fully screened by the free carriers. Our results show this behavior not only in monolayer but also in bilayer and trilayer MoS_2 devices, which indicates that intrinsic scattering mechanisms limit the device performance at low temperatures. The increase in saturation mobility with increasing layer number suggests that short-range scatterers are primarily present at the outer surface of the flakes possibly due to exposure to the ambient and solvent. It should be noted that despite the high concentration of ions, which are effectively charged impurities at the surface of the MoS_2, the low temperature mobility remains nearly constant with top gate bias. This observation suggests that the contribution of long-range scatterers (e.g. charged impurities) at the interface is less dominant compared to short-range scatterers (i.e. structural defects and fully screened charged impurities in the material) in this regime[18,28]. For temperatures above 100 K, the mobility decreases rapidly due to electron-phonon scattering, which can be described by a power law dependence $\mu \sim T^{-\gamma}$. We found that while the Y factor is nearly constant with back gate voltage (Figure 4e), it is strongly dependent on top gate voltage. In bilayer MoS_2, it increases from 1.94 to 2.85 with increasing V_{tg} from 1.65 to 3 V (Figure 4f), similar to the trends observed in previous studies[18,21].

In summary, we show that dual gating of mono- and few-layer MoS_2 using ion gel allows access to a wide range of carrier densities. We demonstrate low device resistivities of 1 kΩ and 420 Ω in mono- and bilayer devices at low temperatures, respectively. The analysis of the dual gating behavior of the devices reveals that the gate coupling is strongly dependent on the doping level and the number of layers. From the coupling ratios, we estimate the quantum capacitance to be on the order of 1 μF/cm^2 for all devices. Our transport results further shed light on the factors limiting carrier mobility in these materials in the highly conducting regime.

Methods

Atomically thin flakes of MoS_2 sheets were mechanically exfoliated from bulk crystals (SPI supplies) and subsequently deposited onto silicon substrate with 300 nm thermal SiO_2. Pure gold contacts (50 nm) for source, drain, and side gate electrodes were fabricated using standard electron beam lithography and thermal evaporation. After lift-off, all devices were annealed in nitrogen atmosphere at 200°C for 2 hours. The ion gel solution was prepared by mixing the polymer PS-PMMA-PS and the ionic liquid EMIM-TFSI (Figure 1c) into an ethyl propionate solvent (weight ratio of polymer: ionic liquid: solvent = 0.7 : 9.3 : 90)[43]. A film of this solution was spin-coated onto the devices and dehydrated in nitrogen gas for an hour to remove molecular moisture. Transport measurements were performed in vacuum inside a Helium 4 cryostat with variable temperature insert.

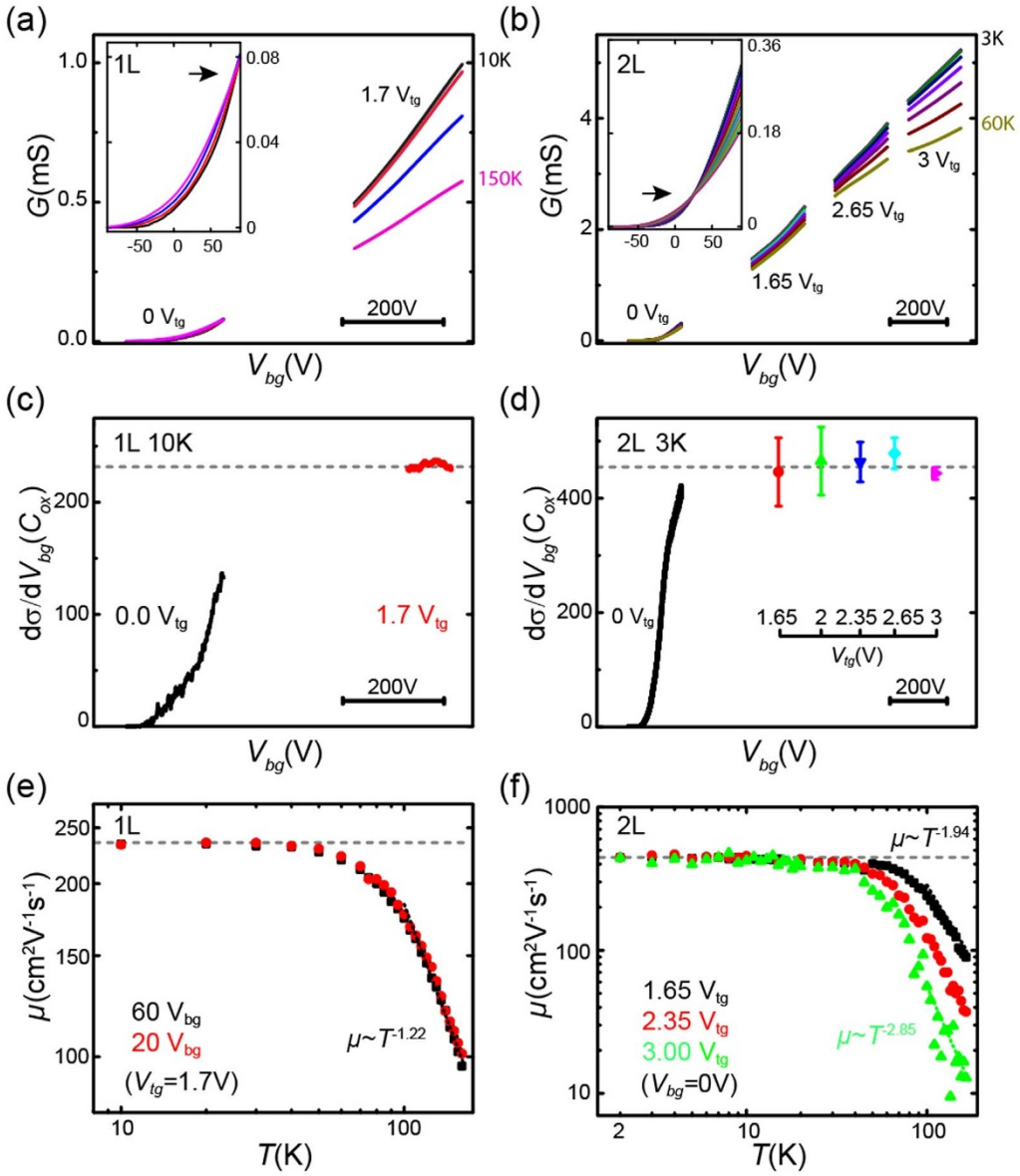

Figure 4 | Transport characteristics at high charge carrier densities. (a, b) Transfer curves of mono- and bilayer samples based on back gate sweeps at different top gate biases. The curves are displaced horizontally to highlight the linear regime where mobility saturates. The arrows in the insets of (a) and (b) indicate the metal-insulator transition point. (c, d) Differential conductivity in units of the oxide capacitance at low temperature as a function of back gate voltages at different top gate biases. Error bars are obtained from the variation of the mobility values as a function of the back gate voltages. (e, f) Temperature dependence of field effect mobility for mono- and bilayer devices. Power law fits are shown to highlight the changes in the phonon damping factors.

1. Novoselov, K. S. *et al.* Two-dimensional atomic crystals. *PNAS* **102**, 10451–10453 (2005).
2. Wang, Q. H., Kalantar-Zadeh, K., Kis, A., Coleman, J. N. & Strano, M. S. Electronics and optoelectronics of two-dimensional transition metal dichalcogenides. *Nat. Nano.* **7**, 699–712 (2012).
3. Radisavljevic, B., Radenovic, A., Brivio, J., Giacometti, V. & Kis, A. Single-layer MoS_2 transistors. *Nat. Nano.* **6**, 147–150 (2011).
4. Wang, H. *et al.* Integrated Circuits Based on Bilayer MoS_2 Transistors. *Nano Lett.* **12**, 4674–4680 (2012).
5. Yu, L. *et al.* Graphene/MoS_2 Hybrid Technology for Large-Scale Two-Dimensional Electronics. *Nano Lett.* **14**, 3055–3063 (2014).
6. Radisavljevic, B., Whitwick, M. B. & Kis, A. Integrated circuits and logic operations based on single-layer MoS_2. *ACS Nano* **5**, 9934–9938 (2011).
7. Wang, H. *et al.* Large-scale 2D electronics based on single-layer MoS_2 grown by chemical vapor deposition. Paper presented at *International Electron Devices Meeting (IEDM) 2012, San Francisco C.A., IEEE* 4.6.1–4.6.4, DOI:10.1109/IEDM.2012.6478980 (2012, Dec. 12–13).
8. Roy, K. *et al.* Graphene-MoS_2 hybrid structures for multifunctional photoresponsive memory devices. *Nat. Nano.* **8**, 826–830 (2013).
9. Baugher, B. W. H., Churchill, H. O. H., Yang, Y. & Jarillo-Herrero, P. Optoelectronic devices based on electrically tunable p-n diodes in a monolayer dichalcogenide. *Nat. Nano.* **9**, 262–267 (2014).
10. Yu, W. J. *et al.* Highly efficient gate-tunable photocurrent generation in vertical heterostructures of layered materials. *Nat. Nano.* **8**, 952–958 (2013).
11. Das, S., Chen, H.-Y., Penumatcha, A. V. & Appenzeller, J. High Performance Multilayer MoS_2 Transistors with Scandium Contacts. *Nano Lett.* **13**, 100–105 (2012).
12. Neal, A., Liu, H., Gu, J. & Ye, P. Metal contacts to MoS_2: A two-dimensional semiconductor. Paper presented at *70th Annual Device Research Conference (DRC), University Park T.X., IEEE*, 65–66, DOI: 10.1109/DRC.2012.6256928 (2012, Jun. 18–20).
13. Ghatak, S., Pal, A. N. & Ghosh, A. Nature of Electronic States in Atomically Thin MoS_2 Field-Effect Transistors. *ACS Nano* **5**, 7707–7712 (2011).
14. Late, D. J., Liu, B., Matte, H. S. S. R., Dravid, V. P. & Rao, C. N. R. Hysteresis in Single-Layer MoS_2 Field Effect Transistors. *ACS Nano* **6**, 5635–5641 (2012).
15. Zhu, W. *et al.* Electronic transport and device prospects of monolayer molybdenum disulphide grown by chemical vapour deposition. *Nat. Commun.* **5**, 3087 (2014).

16. Li, S.-L. *et al.* Thickness-Dependent Interfacial Coulomb Scattering in Atomically Thin Field-Effect Transistors. *Nano Lett.* **13**, 3546–3552 (2013).
17. Liu, H. & Ye, P. D. MoS_2 Dual-Gate MOSFET with Atomic-Layer-Deposited Al_2O_3 as Top-Gate Dielectric. *IEEE Elec. Dev. Lett.* **33**, 546–548 (2012).
18. Radisavljevic, B. & Kis, A. Mobility engineering and a metal–insulator transition in monolayer MoS_2. *Nat. Mater.* **12**, 815–820 (2013).
19. Zhou, W. *et al.* Intrinsic Structural Defects in Monolayer Molybdenum Disulfide. *Nano Lett.* **13**, 2615–2622 (2013).
20. Ghorbani-Asl, M., Enyashin, A. N., Kuc, A., Seifert, G. & Heine, T. Defect-induced conductivity anisotropy in MoS_2 monolayers. *Phys. Rev. B* **88**, 245440 (2013).
21. Schmidt, H. *et al.* Transport Properties of Monolayer MoS_2 Grown by Chemical Vapor Deposition. *Nano Lett.* **14**, 1909–1913 (2014).
22. McDonnell, S., Addou, R., Buie, C., Wallace, R. M. & Hinkle, C. L. Defect-Dominated Doping and Contact Resistance in MoS_2. *ACS Nano* **8**, 2880–2888 (2014).
23. Qiu, H. *et al.* Hopping transport through defect-induced localized states in molybdenum disulphide. *Nat. Commun.* **4**, 2642 (2013).
24. Jariwala, D. *et al.* Band-like transport in high mobility unencapsulated single-layer MoS_2 transistors. *Appl. Phys. Lett.* **102**, 173107 (2013).
25. Wu, J. *et al.* Large Thermoelectricity via Variable Range Hopping in Chemical Vapor Deposition Grown Single-Layer MoS_2. *Nano Lett.* **14**, 2730–2734 (2014).
26. Baugher, B. W. H., Churchill, H. O. H., Yang, Y. & Jarillo-Herrero, P. Intrinsic Electronic Transport Properties of High-Quality Monolayer and Bilayer MoS_2. *Nano Lett.* **13**, 4212–4216 (2013).
27. Ye, J. T. *et al.* Superconducting Dome in a Gate-Tuned Band Insulator. *Science* **338**, 1193–1196 (2012).
28. Ma, N. & Jena, D. Charge Scattering and Mobility in Atomically Thin Semiconductors. *Phys. Rev. X* **4**, 011043 (2014).
29. Kaasbjerg, K., Thygesen, K. S. & Jauho, A.-P. Acoustic phonon limited mobility in two-dimensional semiconductors: Deformation potential and piezoelectric scattering in monolayer MoS_2 from first principles. *Phys. Rev. B* **87**, 235312 (2013).
30. Kaasbjerg, K., Thygesen, K. S. & Jacobsen, K. W. Phonon-limited mobility in n-type single-layer MoS_2 from first principles. *Phys. Rev. B* **85**, 115317 (2012).
31. Lembke, D. & Kis, A. Breakdown of High-Performance Monolayer MoS_2 Transistors. *ACS Nano* **6**, 10070–10075 (2012).
32. Sundaram, R. S. *et al.* Electroluminescence in Single Layer MoS_2. *Nano Lett.* **13**, 1416–1421 (2013).
33. Jena, D. & Konar, A. Enhancement of Carrier Mobility in Semiconductor Nanostructures by Dielectric Engineering. *Phys. Rev. Lett.* **98**, 136805 (2007).
34. Ye, J. *et al.* Accessing the transport properties of graphene and its multilayers at high carrier density. *PNAS* **108**, 13002–13006 (2011).
35. Jo, S., Ubrig, N., Berger, H., Kuzmenko, A. B. & Morpurgo, A. F. Mono- and Bilayer WS_2 Light-Emitting Transistors. *Nano Lett.* **14**, 2019–2025 (2014).
36. Efetov, D. K. & Kim, P. Controlling Electron-Phonon Interactions in Graphene at Ultrahigh Carrier Densities. *Phys. Rev. Lett.* **105**, 256805 (2010).
37. Efetov, D. K., Maher, P., Glinskis, S. & Kim, P. Multiband transport in bilayer graphene at high carrier densities. *Phys. Rev. B* **84**, 161412 (2011).
38. Perera, M. M. *et al.* Improved Carrier Mobility in Few-Layer MoS_2 Field-Effect Transistors with Ionic-Liquid Gating. *ACS Nano* **7**, 4449–4458 (2013).
39. Braga, D., Gutiérrez Lezama, I., Berger, H. & Morpurgo, A. F. Quantitative Determination of the Band Gap of WS_2 with Ambipolar Ionic Liquid-Gated Transistors. *Nano Lett.* **12**, 5218–5223 (2012).
40. Lin, M.-W. *et al.* Mobility enhancement and highly efficient gating of monolayer MoS 2 transistors with polymer electrolyte. *J. of Phys. D* **45**, 345102 (2012).
41. Zhang, Y. J., Ye, J. T., Yomogida, Y., Takenobu, T. & Iwasa, Y. Formation of a Stable p–n Junction in a Liquid-Gated MoS_2 Ambipolar Transistor. *Nano Lett.* **13**, 3023–3028 (2013).
42. Zhang, Y., Ye, J., Matsuhashi, Y. & Iwasa, Y. Ambipolar MoS_2 Thin Flake Transistors. *Nano Lett.* **12**, 1136–1140 (2012).
43. Pu, J. *et al.* Highly Flexible MoS_2 Thin-Film Transistors with Ion Gel Dielectrics. *Nano Lett.* **12**, 4013–4017 (2012).
44. Zhang, Y. J., Oka, T., Suzuki, R., Ye, J. T. & Iwasa, Y. Electrically Switchable Chiral Light-Emitting Transistor. *Science* **344**, 725–728 (2014).
45. Lee, C. *et al.* Anomalous Lattice Vibrations of Single- and Few-Layer MoS_2. *ACS Nano* **4**, 2695–2700 (2010).
46. Mak, K. F., Lee, C., Hone, J., Shan, J. & Heinz, T. F. Atomically Thin MoS_2: A New Direct-Gap Semiconductor. *Phys. Rev. Lett.* **105**, 136805 (2010).
47. Kim, S. *et al.* High-mobility and low-power thin-film transistors based on multilayer MoS_2 crystals. *Nat. Commun.* **3**, 1011 (2012).
48. Yoon, Y., Ganapathi, K. & Salahuddin, S. How Good Can Monolayer MoS_2 Transistors Be? *Nano Lett.* **11**, 3768–3773 (2011).
49. Uesugi, E., Goto, H., Eguchi, R., Fujiwara, A. & Kubozono, Y. Electric double-layer capacitance between an ionic liquid and few-layer graphene. *Sci. Rep.* **3**, 1595 (2013).

Acknowledgments

G.E. acknowledges Singapore National Research Foundation for funding the research under NRF Research Fellowship (NRF-NRFF2011-02) and Graphene Research Centre. T.T. was partially supported by the Funding Program for the Next Generation of World-Leading Researchers and Grants-in-Aid from MEXT (26107533 "Science of Atomic Layers" and 25000003 "Specially Promoted Research"). B. O. acknowledges support by the Singapore Millenium Foundation-NUS Research Horizon award (R-144-001-271-592, R-144-001-271-646) and the NRF-CRP award (R-144-000-295-281).

Author contributions

G.E. supervised the project, G.E. and H.S. designed the experiment, L.C. and S.W. prepared the samples, J.P. and T.T. supplied the ion gel and advised on the usage, L.C. and H.S. performed the measurements, G.E., L.C. and H.S. analysed the data. L.C., H.S., J.P., S.W., B.O., T.T. and G.E. discussed the results and contributed in writing the manuscript. All authors have given approval to the final version of the manuscript.

Additional information

Supplementary information accompanies this paper at http://www.nature.com/scientificreports

Competing financial interests: The authors declare no competing financial interests.

How to cite this article: Chu, L. *et al.* Charge transport in ion-gated mono-, bi-, and trilayer MoS_2 field effect transistors. *Sci. Rep.* **4**, 7293; DOI:10.1038/srep07293 (2014).